BISMUTH FERRITE POWDERS PREPARED BY MICROWAVE-ASSISTED HYDROTHERMAL METHOD

Vasile-Adrian SURDU[1]*, Yaohui WANG[2], Alexandra Cătălina BÎRCĂ[1], Eugenia TANASĂ[1], Ecaterina ANDRONESCU[1]

$BiFeO_3$ powders were synthetized by a fast, reproducible and environmental-friendly microwave-assisted hydrothermal method. The aim of the study is the investigation of increased pressure and different mineralizer concentration on the reaction mechanism, morphology of the particles and magnetic behavior. X-ray diffraction, Field-Emission Scanning Electron Microscopy, Raman spectroscopy and Vibrating Sample Magnetometry showed the successful preparation of $BiFeO_3$ powders at 200°C and 40 bar for 1 h. Particle size was between 1.15 and 5.35 μm. Morphology of particles and aggregates as well as magnetic behavior depend on the concentration of KOH mineralizer.

Keywords: $BiFeO_3$, microwave-assisted hydrothermal, magnetic behavior.

1. Introduction

Multifunctional multiferroic materials that combine ferroelectricity, ferromagnetism and in some cases ferroelasticity have become a challenge both for scientifical and industrial advance. The applications of such materials include photocatalysis [1–3], photocatalytic hydrogen generation [4], gas sensor [5], actuators [6], data storage [7], spintronic devices [8], microwave absorption [9] or magnetic localized dose enhancement in radiotherapy and imaging [10].

One of the most studied material that has coupled electric, magnetic and structural order parameters that results in simultaneous ferroelectricity and antiferromagnetism is $BiFeO_3$. Extensive efforts to obtain single phase $BiFeO_3$ by solid-state reaction without secondary phases was proved to be difficult if not impossible [11–13]. In this view, alternative soft-chemical routes such as sol-gel method [14–16], ultrasonication technique [17], microemultion technique [18] and hydrothermal process [19] have been developed.

Microwave-assisted hydrothermal method is a combination of the hydrothermal and microwave methods, fulfilling the advantages of microwaves and water heat [20]. $BiFeO_3$ synthesis by this method was carried out using NaOH and KOH mineralizers [21–24]. The research aimed the influence of several

[1] Faculty of Applied Chemistry and Materials Science, University POLITEHNICA of Bucharest
[2] ENSIL-ENSCI Limoges, FRANCE
*corresponding author: e-mail: ecaterina.andronescu@upb.ro (Ecaterina ANDRONESCU)

parameters, like mineralizer concentration, concentration of the precursors, temperature and time of treatment. To the best of our knowledge, there is no study regarding microwave-assisted hydrothermal synthesis of $BiFeO_3$ particles at a pressure higher than the vapor pressure of water (≈15 bar at 200°C).

The aim of the present study is to investigate the influence of the mineralizer under increased pressure of 40 bar in the formation mechanism of $BiFeO_3$ particles for various (4 – 14 M) KOH concentrations.

2. Materials and methods

$BiFeO_3$ particles were prepared by microwave assisted hydrothermal method. The chemical reagents used in the present work were $Bi(NO_3)_3 \cdot 5H_2O$, $Fe(NO_3)_3 \cdot 9H_2O$ and KOH. All the reagents were purchased from SigmaAldrich and were of analytical grade. Firstly, bismuth nitrate and iron nitrate were dissolved in distilled water. Then, KOH was added slowly to the Bi-Fe solution to coprecipitate Bi^{3+} and Fe^{3+} ions under constant stirring until a brown precipitate was obtained. KOH concentration was varied from 6M to 14 M. The suspension was poured into a Teflon-lined stainless-steel vessel for microwave-assisted hydrothermal treatment in Milestone Synthwave equipment in different conditions. One batch was treated at 150°C for 1 h, under 40 bar pressure and the other was treated at 200°C for 1 h, under 40 bar pressure. Then, the obtained powders were filtered, washed with distilled water until pH = 7 and dried at 60°C for 12 h.

Phase analysis was performed by X-ray diffraction (PANalytical Empyrean) using Ni-filtered CuKα radiation (λ = 1.5418 Å) after precipitation and microwave-assisted hydrothermal processes. XRD patterns were measured in 2θ range of 10-80° with a step size 0.02° and a counting time per step of 255 s. Phase content and unit cell parameters were obtained through Rietveld refinement in HighScore Plus 3.0.e software. Local symmetry was determined by Raman spectrometry (Horiba LabRAM HR Evolution) with 514 nm Argon ion laser in 50-700 cm^{-1} spectral range. Morphology was studied by Scanning Electron Microscopy with field emission gun (FEI Quanta Inspect F50) at an accelerating voltage of 30 kV. Vibrating sample magnetometry (LakeShore 7404-s VSM) investigated the magnetic behavior of the processed powders.

3. Results and discussion

The influence of KOH concentration in the precursor solution and hydrothermal treatment was studied in what concerns the phase composition after coprecipitation step and microwave-assisted hydrothermal treatments. Fig. 1 illustrates the XRD patterns after coprecipitation.

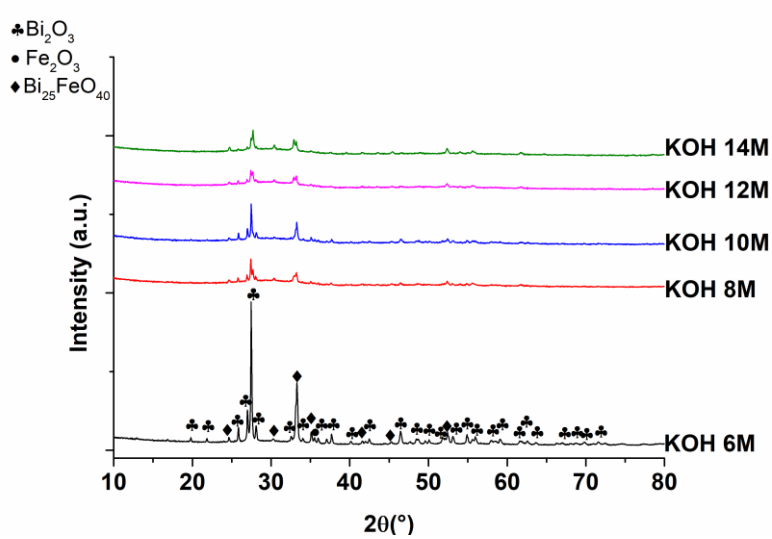

Fig. 1. XRD patterns of powders after coprecipitation step for various concentrations of KOH: 6M, 8M, 10M, 12M and 14M

Peak profiles show a lower degree of crystallinity as the KOH concentration increases, which is observed due to the broadening of the peaks and decrease of intensity. Phase composition analysis showed obtaining α-Bi_2O_3 (ICDD PDF4+ 04-003-2034 [25]), α-Fe_2O_3 (ICDD PDF4+ 04-015-9576 [26]) and $Bi_{25}FeO_{40}$ (ICDD PDF4+ 00-046-041).

Microwave-assisted hydrothermal treatment at 150°C and 40 bar for 1 h promoted the reaction between the phases obtained by coprecipitation. Fig. 2 depicts XRD patterns measured on the powders obtained after the treatment.

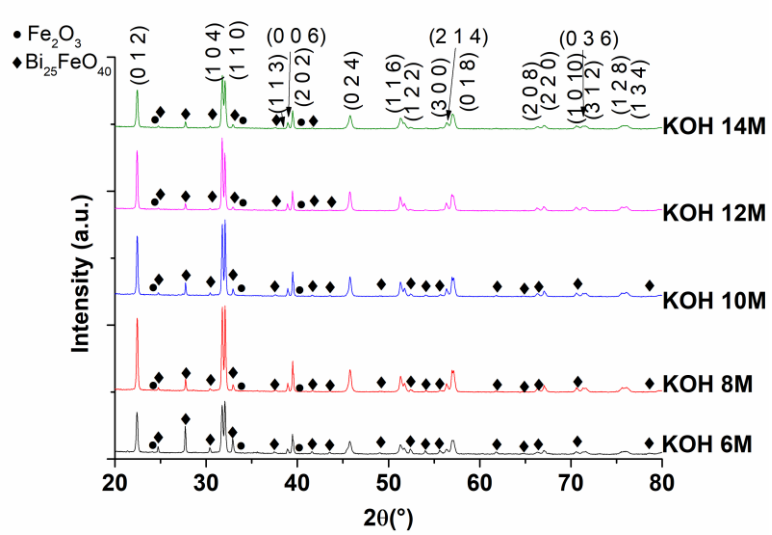

Fig. 2. XRD patterns of $BiFeO_3$ powders synthesized at 150°C and 40 bar for 1 h

At this stage, independent of KOH concentration, $BiFeO_3$ with rhombohedral distorted perovskite structure is formed (ICDD PDF4+ 01-081-9728 [27]). Besides, there are still unreacted α-Fe_2O_3 and $Bi_{25}FeO_{40}$. The amount of secondary phases decreases with the increase of KOH concentration, evidenced by the decrease of the intensities of the corresponding phases.

The powders obtained by treatment at 200°C and 40 bar for 1 h show single phase composition starting with a concentration of 8 M KOH (Fig. 3).

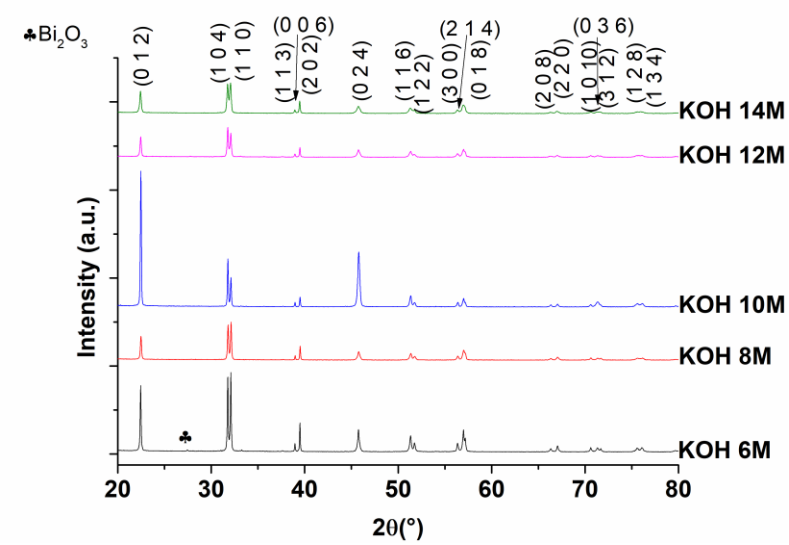

Fig. 3. XRD patterns of $BiFeO_3$ powders synthesized at 200°C and 40 bar for 1 h

At a concentration of KOH of 6 M, there is also present a diffraction peak with a low intensity at 2θ = 27.45°, which most probably corresponds to Bi_2O_3. This may occur because of different solubility of Bi^{3+} and Fe^{2+} when the concentration of KOH is low [28]. As the concentration of KOH increases from 8 M to 14 M, the profiles of the peaks show a decrease in the crystallinity degree. Interestingly, at 10 M one can notice a preferential orientation along [012] direction which is evidenced by the increase of intensity of the peaks corresponding to (012) and (024) crystallographic planes.

XRD patterns were further refined by Rietveld method in order to assess quantitatively the phase composition and to determine the unit cell parameters for the powders synthetized at 200°C. Fig. 4 shows the evolution of composition versus KOH concentration after coprecipitation step (CP) and microwave-assisted hydrothermal treatments (M-H). By looking at the trends, it may be concluded that both the concentration of KOH and the treatment temperature have a crucial role in what concerns obtaining $BiFeO_3$ powders without secondary phases. Besides, this representation also suggests the reaction pathway. At room temperature, Bi^{3+} and Fe^{3+} ions react with KOH to form crystalline Bi_2O_3, Fe_2O_3

and an intermediate sillenite-type crystal $Bi_{25}FeO_{40}$. When increasing the temperature and pressure in the hydrothermal reactor, several processes may occur. On the one hand, the reaction between Bi_2O_3 and Fe_2O_3 as well as the reaction between $Bi_{25}FeO_{40}$ and Fe_2O_3 is promoted. The concentration of KOH also plays a crucial role because the higher the concentration the lower the crystallinity degree, which speeds the reaction between components. On the other hand, at 200°C there is a competition between crystallization and dissolution for Bi^{3+}, which may affect the stoichiometry in $BiFeO_3$.

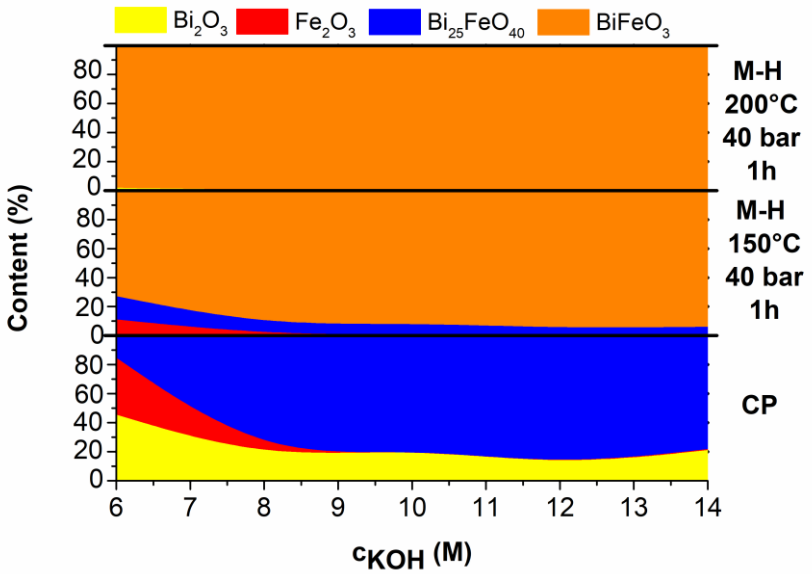

Fig. 4. Phase composition evolution after coprecipitation (CP) and microwave-hydrothermal treatment at 150°C and 200°C

The evolution of unit cell parameters, crystallite size, microstrain and crystallinity degree for different concentrations of KOH obtained from Rietveld refinement are shown in Table 1. The values of R_{exp}, R_p, R_{wp} and χ^2 parameters indicated a high quality data fit.

When increasing the concentration of KOH from 6 M to 8M, *a*, *c* and *V* increase, as a result of incorporation of Bi^{3+} ions in the perovskite lattice, as in the case of 6 M there is also 1.5% Bi_2O_3 secondary phase. As the concentration further increases, the trend for unit cell parameter *c* is a decreasing one, except the 10 M concentration where is present a preferential orientation on [012] direction as stated before. The degree of crystallinity decreases with the increase of concentration, except the case of 10 M where the orientation promotes faster crystallization. Average crystallite size and microstrain vary as expected. Thus,

the average crystallite size is decreasing and the microstrain is increasing when increasing the concentration of KOH from 6 to 14 M.

Table 1

Unit cell parameters, average crystallite size, microstrain and crystallinity degree for powders treated at 200°C

	6 M	8 M	10 M	12 M	14 M
a (Å)	5.580660 ± 0.000120	5.582918 ± 0.000225	5.582330 ± 0.000269	5.581063 ± 0.000292	5.583564 ± 0.000295
c (Å)	13.872090 ± 0.000334	13.876740 ± 0.000616	13.879020 ± 0.000845	13.872740 ± 0.000817	13.868180 ± 0.000831
V (Å^3)	374.1483	374.5766	374.5589	374.2198	374.4322
< *D* > (nm)	71.52 ± 35.89	44.71 ± 24.42	36.21 ± 20.48	35.91 ± 15.48	27.08 ± 12.57
< *S* > (%)	0.12 ± 0.01	0.21 ± 0.04	0.26 ± 0.06	0.25 ± 0.03	0.33 ± 0.05
Crystallinity (%)	65.58	58.04	65.74	56.21	55.90
R_{exp}	4.73345	5.88156	5.13509	5.8494	5.59764
R_p	4.74719	5.33156	8.26663	5.57075	4.63677
R_{wp}	7.16821	8.07722	12.92238	8.01321	7.06300
χ^2	2.29333	1.88599	6.33270	1.87668	1.59209

The powders obtained at 200°C were further investigated in terms of local symmetry, morphology and magnetic behavior.

Raman spectroscopy (Fig. 5) was performed to support Rietveld analysis of the XRD patterns.

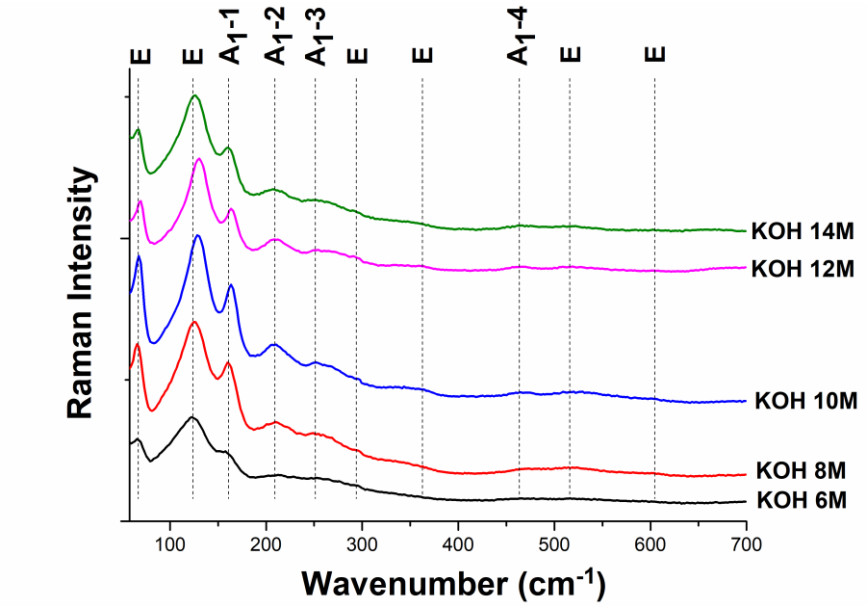

Fig. 5. Raman spectra of $BiFeO_3$ powders synthesized at 200°C

The active Raman modes of $BiFeO_3$ with rhombohedral distorted perovskite structure belonging *R3c* space group may be summarized using the irreducible representation of $\Gamma_{\text{Raman, R3c}} = 4A_1 + 9E$ [29]. A_1-1 and A_1-2 modes are attributed to Bi-O bonds and, in this case, they shift to higher frequency side for 10 M and 12 M KOH concentration. This suggests that the mass of A-site in the perovskite structure is lower comparing to the other structures obtained in different conditions. A possible explanation is that in those cases, there is present a partial dissolution of Bi^{3+} from perovskite lattice.

FE-SEM images, particle size distribution and EDS analysis on $BiFeO_3$ powders obtained at 200°C for 6 M KOH concentration are shown in Fig. 6.

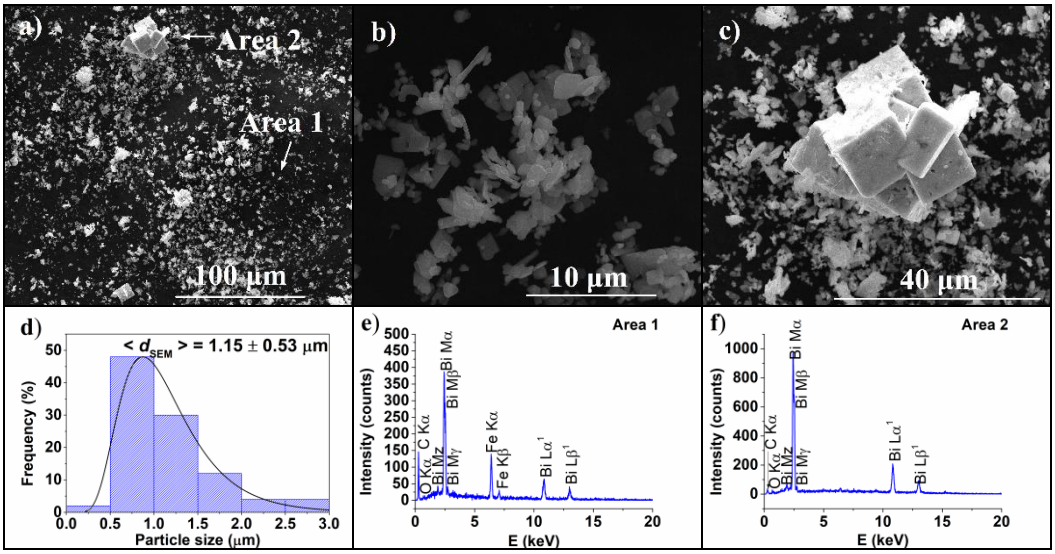

Fig. 6. FE-SEM images a) general view, b), c) details on Area 1 and Area 2, d) particle size distribution, e), f) EDS analysis on Area 1 and Area 2 at 6 M KOH concentration

The general view (Fig. 6 a)) evidence two types of morphologies. Area 1 (Fig. 6 b)) shows particles of 1.15 µm with irregular morphology. EDS spectrum on Area 1 (Fig. 6 e)) confirms the presence of $BiFeO_3$. Area 2 (Fig. 6 c)) is attributed to Bi_2O_3 secondary phase, as in this case the EDS spectrum (Fig. 6 f)) shows no contribution from iron. Bi_2O_3 particles exhibit cubic morphology and a tendency for agglomeration.

The powders prepared at higher KOH concentration of 8, 10, 12 and 14 M consist of aggregates of microcrystalline building units. At 8 M KOH concentration (Fig. 7 a)), the aggregates of flakes building units (Fig. 7 b)) show a cvasi-spherical shape. At 10 M KOH concentration, the cubic building units assemble face to face like the blocks in a Rubik's Cube (Fig. 7 d) and e)) consistent with Suzuki *et al.* findings [30]. With a further increase in the concentration, the building units become more round edged and have an irregular

shape (Fig 7. h) and k)). The aggregates in the case of 12 and 14 M KOH (Fig. 7 f) and j)) concentration show spherical morphology. The average size of building unit decreases with the increase of KOH concentration from 5.35 μm at 8M to 1.57 μm at 14 M. The particle size distribution (Fig. 7 c), f), i) and l)) is single modal lognormal and narrow for 8 and 10 M and single modal but large for 12 and 14 M.

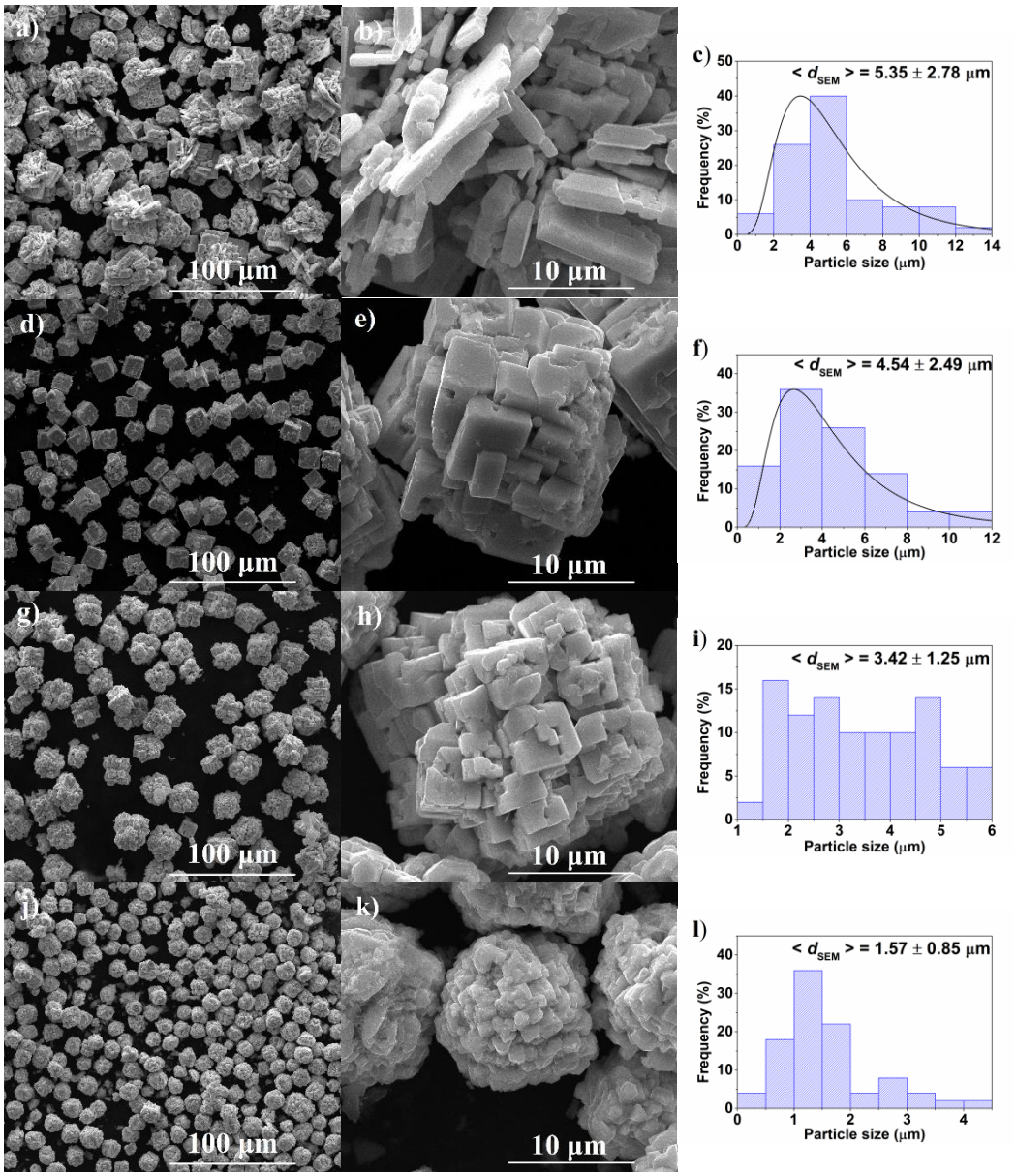

Fig. 7. a), d), g), j) FE-SEM general view, b), e), h), k) FE-SEM detail and c), f), i), l) particle size distribution at 8, 10, 12 and 14 M KOH concentration

Table 2 presents the elemental analysis of $BiFeO_3$ powders synthesized at 200°C. Although EDS is a semi-quantitative analysis and the error bars are relatively large, Bi/Fe ratio determined from these data support Raman investigations. Thus, in the case of 10 and 12 M KOH concentrations, Bi/Fe ratio is 0.95 and, respectively 0.83, which indicate a deficit of Bi^{3+} on the A-site of the distorted perovskite structure.

Table 2

Elemental analysis of $BiFeO_3$ powders synthesized at 200°C

KOH concentration	EDS quantification	O K	Fe K	Bi L	Bi/Fe
8 M	Atomic %	48.61	25.73	25.66	0.99
	Error %	16.61	6.32	9.35	
10 M	Atomic %	51.43	24.9	23.67	0.95
	Error %	16.44	6.35	13	
12 M	Atomic %	52.92	25.66	21.42	0.83
	Error %	15.97	6.15	12.9	
14 M	Atomic %	52.48	24.05	23.47	0.97
	Error %	15.58	6.64	12.47	

Magnetization versus field curves and typical parameters obtained for $BiFeO_3$ powders synthetized at 200°C are shown in Fig. 8 and Table 3.

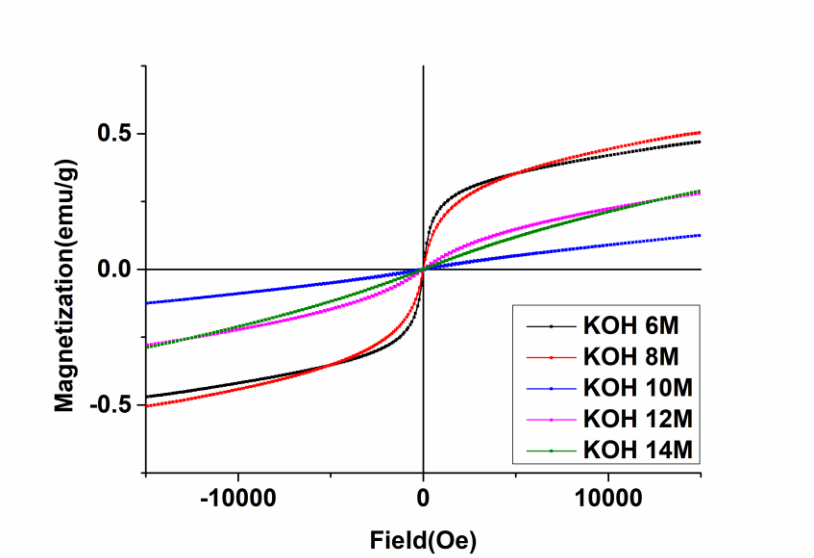

Fig. 8. M-H curves of $BiFeO_3$ powders synthetized at 200°C

For 6 and 8 M KOH concentrations, the curves exhibit a paramagnetic behavior, which we assume that is linked to non-crystalline iron reach phases,

which may not be identified by XRD measurements. At higher concentrations, the curves exhibit typical $BiFeO_3$ antiferromagnetic behavior.

Table 3

H_C, M_S, M_r of $BiFeO_3$ powders synthesized at 200°C

	KOH 6 M	KOH 8 M	KOH 10 M	KOH 12 M	KOH 14 M
H_C	2.2614	3.138	175.84	54.36	43.15
M_S	0.4699	0.5032	0.1035	0.2791	0.2877
M_R	0.0014	0.0011	0.0018	0.0026	0.0011

When assessing the coercitivity (Table 3), it may be noticed that the highest value is obtained for 10 M KOH concentration. This may suggest that preferential orientation observed in crystal growth may have an impact on the magnetic behavior of $BiFeO_3$.

4. Conclusions

Bismuth ferrite powders with micrometer-ranged particles were prepared by microwave-assisted hydrothermal method. The temperature of the hydrothermal treatment and the concentration of KOH are important parameters for obtaining secondary phase free compositions, as evidenced by XRD measurements. After coprecipitation step, the powders consist of Bi_2O_3, Fe_2O_3 and $Bi_{25}FeO_{40}$ in different ratios, dependent on the concentration of KOH. When the concentration increases, the formation of $Bi_{25}FeO_{40}$ intermediate is promoted. When treating the precursor solution under microwave-hydrothermal conditions at 40 bar and 150°C for 1h, the process of $BiFeO_3$ formation is not complete, therefore resulting secondary phases of $Bi_{25}FeO_{40}$ and Fe_2O_3. The trend versus KOH concentration is similar to that observed after coprecipitation step. $BiFeO_3$ particles can be successfully synthesized at 40 bar under microwave-hydrothermal conditions at a temperature of 200°C and a concentration of KOH of at least 8M. At 6M, the composition consisted of 98.5% $BiFeO_3$ and 1.5% Bi_2O_3 as evidenced by Rietveld refinement. Moreover, for the concentration of 10 M KOH, one can notice a preferential orientation along [012] direction. Raman spectroscopy and EDS analysis showed the possibility of controlling Bi/Fe ratio in highly basic solutions. Different solubility of Bi^{3+} and Fe^{3+} in KOH solutions results in a partial dissolution of Bi_2O_3 at 200°C and poor control of Bi/Fe ratio in $BiFeO_3$ at KOH concentrations of 10 and 12 M. Particle and aggregates morphology depicted by FE-SEM investigations showed a tendency to form irregular shaped particles at KOH concentration of 6 M, for which the reaction is not complete. When increasing the concentration, $BiFeO_3$ particles exhibit regular shapes from cubic at 8 M to cvasi-spherical at 14 M. These particles show a high degree of aggregation into uniform shapes and sizes for all concentration between 8 and 14

M. The average size of the building units of aggregates increases from 1.15 μm at 6 M to 5.35 μm at 8 M and then decreases to 1.57 μm at 14 M KOH concentrations. M-H curves characteristics illustrate that Bi/Fe ratio and preferential orientation of crystal growth influence the magnetic behavior of $BiFeO_3$ crystalline powders.

Acknowledgement

Microwave-assisted hydrothermal treatment, SEM and Raman spectroscopy characterizations were possible thanks to Project POSCCE, No.638/12.03.2014.

R E F E R E N C E S

[1]. *Gao, X.; Dai, Y.; Fu, F.; Hua, X*. 2D laminated cylinder-like $BiFeO_3$ composites: Hydrothermal preparation, formation mechanism, and photocatalytic properties. Solid State Sci. **62,** 2016, pp. 6–12.

[2]. *Duan, Q.; Kong, F.; Han, X.; Jiang, Y.; Liu, T.; Chang, Y.; Zhou, L.; Qin, G.; Zhang, X*. Synthesis and characterization of morphology-controllable $BiFeO_3$ particles with efficient photocatalytic activity. *Mater. Res. Bull.* **112**, 2019, pp. 104–108.

[3]. *Li, S.; Zhang, G.; Zheng, H.; Zheng, Y.; Wang, P*. Stability of $BiFeO_3$ nanoparticles via microwave-assisted hydrothermal synthesis in Fenton-like process. Environ. Sci. Pollut. Res. **24**, 2017, pp. 24400–24408.

[4]. *Bera, S.; Ghosh, S.; Shyamal, S.; Bhattacharya, C.; Basu, R.N*. Photocatalytic hydrogen generation using gold decorated $BiFeO_3$ heterostructures as an efficient catalyst under visible light irradiation. Sol. Energy Mater. Sol. Cells **194**, 2019, pp. 195–206.

[5]. *Zhu, K.M.; Ma, S.Y.; Pei, S.T.; Tie, Y.; Zhang, Q.X.; Wang, W.Q.; Xu, X.L*. Preparation, characterizaton and formaldehyde gas sensing properties of walnut-shaped $BiFeO_3$ microspheres. Mater. Lett. **246**, 2019, pp. 107–110.

[6]. *Wang, J.; Neaton, J.B.; Zheng, H.; Nagarajan, V.; Ogale, S.B.; Liu, B.; Viehland, D.; Vaithyanathan, V.; Schlom, D.G.; Waghmare, U. V; et al*. Epitaxial $BiFeO_3$ multiferroic thin film heterostructures. Science **299**, 2003, pp. 1719–1722.

[7]. *Čebela, M.; Zagorac, D.; Batalović, K.; Radaković, J.; Stojadinović, B.; Spasojević, V.; Hercigonja, R*. $BiFeO_3$ perovskites: A multidisciplinary approach to multiferroics. Ceram. Int. **43**, 2017, pp. 1256–1264.

[8]. *Lee, J.H.; Fina, I.; Marti, X.; Kim, Y.H.; Hesse, D.; Alexe, M*. Spintronic functionality of $BiFeO_3$ domain walls. Adv. Mater. **26**, 2014, pp. 7078–7082.

[9]. *Kang, Y.Q.; Cao, M.S.; Yuan, J.; Shi, X.L*. Microwave absorption properties of multiferroic $BiFeO_3$ nanoparticles. Mater. Lett. **63**, 2009, pp. 1344–1346.

[10]. *Rajaee, A.; Wensheng, X.; Zhao, L.; Wang, S.; Liu, Y.; Wu, Z.; Wang, J.; Si-Shen, F*. Multifunctional bismuth ferrite nanoparticles as magnetic localized dose enhancement in radiotherapy and imaging. J. Biomed. Nanotechnol. **14**, 2018, pp. 1159–1168.

[11]. *Rodrigues, H.O.; Pires, G.F.M.; Almeida, J.S.; Sancho, E.O.; Ferreira, A.C.; Silva, M.A.S.; Sombra, A.S.B*. Study of the structural, dielectric and magnetic properties of Bi_2O_3 and PbO addition on $BiFeO_3$ ceramic matrix. J. Phys. Chem. Solids **71**, 2010, pp. 1329–1336.

[12]. *Lufaso, M.W.; Vanderah, T.A.; Pazos, I.M.; Levin, I.; Roth, R.S.; Nino, J.C.; Provenzano,*

V.; Schenck, P.K. Phase formation, crystal chemistry, and properties in the system Bi_2O_3-Fe_2O_3-Nb_2O_5. J. Solid State Chem. **179**, 2006, pp. 3900–3910.

[13]. *Bernardo, M.S.; Jardiel, T.; Peiteado, M.; Caballero, A.C.; Villegas, M.* Reaction pathways in the solid state synthesis of multiferroic $BiFeO_3$. J. Eur. Ceram. Soc. **31**, 2011, pp. 3047–3053.

[14]. *Sankar Ganesh, R.; Sharma, S.K.; Sankar, S.; Divyapriya, B.; Durgadevi, E.; Raji, P.; Ponnusamy, S.; Muthamizhchelvan, C.; Hayakawa, Y.; Kim, D.Y.* Microstructure, structural, optical and piezoelectric properties of $BiFeO_3$ nanopowder synthesized from sol-gel. Curr. Appl. Phys. **17**, 2017, pp. 409–416.

[15]. *Wang, T.; Song, S.H.; Ma, Q.; Ji, S.S.* Multiferroic properties of $BiFeO_3$ ceramics prepared by spark plasma sintering with sol-gel powders under an oxidizing atmosphere. Ceram. Int. **45**, 2019, pp. 2213–2218.

[16]. *Majid, F.; Mirza, S.T.; Riaz, S.; Naseem, S.* Sol-Gel Synthesis of $BiFeO_3$ Nanoparticles. Mater. Today Proc. **2**, 2015, pp. 5293–5297.

[17]. *Basith, M.A.; Ngo, D.T.; Quader, A.; Rahman, M.A.; Sinha, B.L.; Ahmmad, B.; Hirose, F.; Mølhave, K.* Simple top-down preparation of magnetic $Bi_{0.9}Gd_{0.1}Fe_{1-x}Ti_xO_3$ nanoparticles by ultrasonication of multiferroic bulk material. Nanoscale **6**, 2014, pp. 14336–14342.

[18]. *Das, N.; Majumdar, R.; Sen, A.; Maiti, H.S.* Nanosized bismuth ferrite powder prepared through sonochemical and microemulsion techniques. Mater. Lett. **61**, 2007, pp. 2100–2104.

[19]. *Zhang, H.; Kajiyoshi, K.* Hydrothermal synthesis and size-dependent properties of multiferroic bismuth ferrite crystallites. J. Am. Ceram. Soc. **93**, 2010, pp. 3842–3849.

[20]. *Yang, G.; Park, S.J.* Conventional and microwave hydrothermal synthesis and application of functional materials: A review. Materials (Basel). **12**, 2019.

[21]. *Li, S.; Nechache, R.; Davalos, I.A.V.; Goupil, G.; Nikolova, L.; Nicklaus, M.; Laverdiere, J.; Ruediger, A.; Rosei, F.* Ultrafast microwave hydrothermal synthesis of $BiFeO_3$ nanoplates. J. Am. Ceram. Soc. **96**, 2013, pp. 3155–3162.

[22]. *Zheng, Y.Q.; Tan, G.Q.; Miao, H.Y.; Xia, A.; Ren, H.J.* Self-assembly growth of BiFeO3 powders prepared by microwave-hydrothermal method. Mater. Lett. **65**, 2011, pp. 1137–1140.

[23]. *Wang, Z.; Zhu, J.; Xu, W.; Sui, J.; Peng, H.; Tang, X.* Microwave hydrothermal synthesis of perovskite $BiFeO_3$ nanoparticles: An insight into the phase purity during the microwave heating process. Mater. Chem. Phys. **135**, 2012, pp. 330–333.

[24]. *Prado-Gonjal, J.; Villafuerte-Castrejon, M.E.; Fuentes, L.; Moran, E.* Microwave-hydrothermal synthesis of the multiferroic $BiFeO_3$. Mater. Res. Bull. **44**, 2009, pp. 1734–1737.

[25]. *Malmros, G.* The Crystal Structure of α-Bi_2O_3. Acta Chem. Scand. **24**, 1970, pp. 384–396.

[26]. *Hill, A.H.; Jiao, F.; Bruce, P.G.; Harrison, A.; Kockelmann, W.; Ritter, C.* Neutron Diffraction Study of Mesoporous and Bulk Hematite a-Fe_2O_3. Chem. Mater. **20**, 2008, pp. 4891–4899.

[27]. *Kiyanagi, R.; Yamazaki, T.; Sakamoto, Y.; Kimura, H.; Noda, Y.; Ohyama, K.; Torii, S.; Yonemura, M.; Zhang, J.; Kamiyama, T.* Structural and magnetic phase determination of (1 - x)$BiFeO_3$-x$BaTiO_3$ solid solution. J. Phys. Soc. Japan 81, 2012, pp. 1–6.

[28]. *Xu, X.; Xu, Q.; Huang, Y.; Hu, X.; Huang, Y.; Wang, G.; Hu, X.; Zhuang, N.* Control of crystal phase and morphology in hydrothermal synthesis of $BiFeO_3$ crystal. J. Cryst. Growth **437**, 2016, pp. 42–48.

[29]. *Rao, T.D.; Karthik, T.; Asthana, S.* Investigation of structural, magnetic and optical properties of rare earth substituted bismuth ferrite. J. Rare Earths **31**, 2013, pp. 370–375.

[30]. *Suzuki, K.; Tokudome, Y.; Tsuda, H.; Takahashi, M.* Morphology control of $BiFeO_3$ aggregates via hydrothermal synthesis. J. Appl. Crystallogr. **49**, 2016, pp. 168–174.